Quantitative multiplexed analysis of MMP-11 and CD45 in metastatic breast cancer tissues by immunohistochemistry-assisted LA-ICP-MS

Dylan Johnson[1], David Clases[1,2], Maria Luisa Fernández-Sánchez[3], Noemi Eiro[4], Luis O. González[4], Francisco J. Vizoso[4], Philip A. Doble[1], Raquel Gonzalez de Vega[1,2*]

[1]The Atomic Medicine Initiative, University of Technology Sydney, NSW, Australia

[2]TESLA-Analytical Chemistry, Institute of Chemistry, University of Graz, Austria

[3]Department of Physical and Analytical Chemistry, University of Oviedo, Spain

[4]Research Unit, Hospital de Jove Foundation, Gijón, Spain

***Corresponding author: email: raquel.gonzalez-de-vega@uni-graz.at**

ABSTRACT: Breast cancer is the leading cause of cancer death and tremendous efforts are undertaken to limit dissemination and to provide effective treatment. Various histopathological parameters are routinely assessed in breast cancer to provide valuable predictive and prognostic information. MMP-11 and CD45 are tumour associated antigens and increasing evidence support the hypothesis that they are valuable biomarkers to interrogate tumours regarding aggressiveness and metastasis. This paper presents methods for quantitative and multiplexed imaging of MMP-11 and CD45 in breast cancer tissues and investigates their potential for improved cancer characterisation. An immunohistochemistry (IHC)-assisted LA-ICP-MS method was successfully developed and optimised using lanthanide tagged monoclonal antibodies as proxies to investigate distributions and concentrations of breast cancer biomarkers. The labelling degree of antibodies was determined via size exclusion – inductively coupled plasma – tandem mass spectrometry (SEC-ICP-MS/MS) employing on-line calibration via post-column isotope dilution analysis. To calibrate spatial intensity distributions of lanthanides in tissues, gelatine standards were spiked with element standards and analysed in parallel for external calibration. In conjunction with the determined labelling degree, this enabled the translation of lanthanide intensities into concentrations of biomarkers. A k-means clustering method was used to select tissue areas for statistical analysis and mean concentrations were compared for sets of metastatic, non-metastatic and healthy control samples. MMP-11 was expressed in stroma surrounding tumour areas, while CD45 was predominantly found inside tumour areas of high cell density. There was no significant correlation between CD45 and metastasis ($p = 0.70$), however, MMP-11 was significantly upregulated (202%) in metastatic breast cancer compared to non-metastatic ($p = 0.0077$) and control tissues ($p = 0.0087$).

Keywords Element imaging · Immunoassays · Hyphenated techniques · SEC-ICP-MS · Biomarker quantification

Introduction

Breast cancer is the leading worldwide cause of cancer death in women [1]. A key characteristic of breast cancer is its propensity for invasion and metastasis which necessitates early detection and characterisation for optimum treatment outcomes [2]**.** Tumour size, histological type, mitotic index, presence of necrosis, vascular invasion, status of hormonal receptors and assessments of axillary lymph nodes are typically used for diagnosis, treatment and prognosis [3]**.** These clinical metrics may be augmented by inclusion of recently discovered biomarkers that have the potential to provide additional diagnostic and prognostic insights [4]**.**

The tumour microenvironment plays a significant role in disease progression by facilitating the transformation of epithelial cells into malignant neoplasms [7,8]. This microenvironment consists of dynamically interacting cell populations and biomolecules such as cytokines, stroma, endothelium, fibroblasts, and inflammatory cells [6].

Matrix metalloproteinases (MMPs) belong to a family of zinc-dependent endopeptidases that aid tissue remodelling by degradation of the extracellular matrix [5]**,** a critical factor for carcinogenesis and metastasis of breast cancer tumours. MMP-11 was first identified in stromal cells in breast carcinomas and is a member of the stromelysin subgroup (stromelysin-3) [9]**.** Tumours and surrounding stromal cells are known to express MMP-11 [10], and together with other MMPs are implicated in breast cancer pathogenesis [11]. Estrogen receptor (ER) and human epidermal growth factor receptor 2 (HER2) status has been linked to MMP-11 expression in both tumours and stromal fibroblasts [12]**,** suggesting that MMP-11 may be involved in signalling transduction or other unknown biochemical pathways with influences beyond its primary proteolysis activity [6]**.** Min *et al.* demonstrated that MMP-11 expression was significantly related to standard clinicopathological assessments and was useful for prediction of disease outcome in patients with invasive ductal carcinoma, which accounts for 70-80% of breast cancer cases [12]**.** Furthermore, recent studies by Gonzalez de Vega *et al.* [13,14] and Eiro *et al.* [15] showed that MMP-11 expression in stromal cells was a potentially important biomaker for enhanced patient stratification.

CD45 (PTPRC) is an enzyme of the protein tyrosine phosphatase (PTP) family. PTPs are signalling molecules that regulate a variety of cellular processes, including cell growth, differentiation, mitotic cycle, and oncogenic transformation. CD45 is a type I transmembrane protein that is present in all differentiated hematopoietic cells [16]. It has been shown to be an essential regulator of T- and B-cell antigen receptor signalling. Caldwell and Patterson observed correlations between the CD45 antigen,

and the putative stages of cell differentiation for malignant B-cells at earlier stages of malignancies, however a progressive loss of CD45 occurred at later stages [17]. Interference in the function of CD45 regulatory processes may also contribute to the malignancy of breast cancer [18,19].

Routine clinical methods for breast cancer detection and classification are based on enzyme or fluorophore linked immunoassays, which enable visual interpretation by trained personal. However, these techniques are limited by sensitivity and accuracy and are difficult to multiplex. Discordance of subjective histopathological grading may also impact tumour classification and treatment efficacy and prognosis [20]. A relatively new direction for biomarker measurement is the application of elemental bio-imaging (EBI) by laser ablation - inductively coupled plasma - mass spectrometry (LA-ICP-MS) to produce quantitative images of elemental distributions in biological tissues [21]. LA-ICP-MS has previously been employed to interrogate elemental distributions in tumours and their microenvironments [22,23]. Quantification of elemental distributions is either possible by the parallel analysis of spiked standards or via on-line calibration techniques [24,25]. The implementation of immunohistochemical methods into LA-ICP-MS workflows expanded the capabilities beyond determination of elements by targeting antibodies labelled with metals that serve as proxies for indirect quantification of bio-indicative antigen/proteins [21]. As such, LA-ICP-MS is an ideal imaging modality for applications that require both metallomic and proteomic analyses [26,27].

Isotopically enriched lanthanide polymer tags for labelling antibodies are commercially available and has been applied to multiplexed analysis of up to 40 biomolecules in a single acquisition [28]. The labelling process involves conjugation of one or more polymer tags of variable sizes and number of isotopes to each antibody. Accordingly, characterisation of the conjugate is necessary to determine labelling degree and to ensure reproducible quantitative analyses. A suitable approach is the hyphenation of size exclusion chromatography (SEC) and ICP-MS(/MS) to separate and detect labelled antibodies. Post-column isotope dilution is preferred to simultaneously determine absolute concentrations of both antibodies and labelled isotopes, as well as labelling efficiencies [25].

This paper presents a quantitative multiplexed IHC-LA-ICP-MS method for spatially resolved analysis of MMP-11 and CD45 in metastatic, non-metastatic and healthy breast tissues. Comparisons of these tissues supported previous findings of the prognostic potential of MMP-11 as an indicator of metastatic disease.

Experimental

Chemicals and consumables

High-purity ICP-MS standard calibration solutions of 10 mg L^{-1} Nd, Eu and S were purchased from Choice Analytical (Thornleigh NSW, Australia). Enriched ^{34}S (91.24%) was obtained from ISC Science (Oviedo, Spain). The concentration of sulphur in this solution was determined by reverse isotope dilution analysis with a certified standard containing S with natural isotopic abundance. Ultra-pure water (18.2 MΩ cm) was obtained from a Sartorius 611 arium® pro water generation system (Sartorius Lab Instruments GmbH & Co. KG, Goettingen, Germany). Ammonium acetate (99.999% purity) was used to prepare the SEC eluent and was purchased from Sigma-Aldrich (Castle Hill, NSW, Australia).

Monoclonal anti-MMP11 (MAB3657) and anti-CD45 (MAB1430) antibodies were obtained from In-Vitro Technologies (VIC, Australia) and labelled with ^{142}Nd (97.95%) and ^{170}Er (96.92%), respectively, using the MAXPAR® antibody conjugation kits (Fluidigm; formerly DVS Sciences, San Francisco, CA) according to the manufacturer's standard protocol (version 4 06/13). Xylene and ethanol were obtained from ChemSupply (Gillman, SA, Australia). Bovine serum albumin (BSA), Triton X-100, normal goat serum (NGS), tris buffered saline (TBS) and phosphate buffered saline (PBS) were obtained from Sigma-Aldrich (Castle Hill, NSW, Australia).

Sample collection

Paraffin-embedded human breast cancer and healthy breast samples were obtained from the Hospital de Jove Foundation (Gijón, Spain). The study adheres to national regulations and was approved by the Hospital de Jove Foundation Ethics and Investigation Committee (PI02/2018). H&E-stained tissue sections of all cancer samples were provided to locate and characterise the areas of interest within the tissue.

Additionally, colorimetric IHC standard staining of MMP-11, ER, PR and HER2 was performed in consecutive breast tissue sections following a protocol described by Eiró *et al*. [15] to determine the presence of these biomarkers within the tissue. Each sample was pathologically graded and awarded a score of 0 (negative) or 1 (positive). Clinicopathological characteristics of the breast tissue samples analysed in this study are listed in Table S1 of the Electronic Supplementary Material (ESM).

Tissue staining procedure for LA-ICP-MS analyses

Breast tissue samples were provided as formalin-fixed paraffin-embedded (FFPE) sections. Serial 5-µm sections were cut using a microtome (Leica Microsystems GmbH, Wetzlar, Germany) and transferred to adhesive-coated slides. Paraffin-embedded slides were first heated in a 60°C oven for 60-90 minutes. After baking, each slide was hydrated by incubation in the following solutions for five minutes, respectively: two xylene solutions, 100% ethanol, 95% ethanol and 5% pure water, 50% ethanol and 50% pure water. Subsequently, slides were then kept in PBS (1x) until needed for staining.

For the main staining procedure, a hydrophobic border was drawn around the tissue, and a blocking solution comprising of 1% (w/v) BSA, 0.3% Triton X-100, 3% (v/v) NGS in PBS (1x) was applied for 45 minutes in a sealed environment mitigating unspecific binding of antibodies. The blocking solution was removed and the anti-CD45 antibody, diluted in a 1:50 mixture in blocking solution, was added onto the tissue section and incubated for two hours. Afterwards, the tissue was washed with gentle agitation three times for five minutes in TBS (1x). Subsequently, the anti-MMP-11 antibody was applied in the same way at a 1:100 dilution. After antibody incubation, the tissue was washed and left to dry before storage and LA-ICP-MS analysis.

Instrumentation

Antibody characterisation was carried out by SEC-ICP-MS/MS. SEC was performed using an ACQUITY UPLC Protein BEH SEC column with the dimensions 1.7 µm, 2.1 x 150

mm (pore size 200 Å, MW range 10-450 kDa; Waters, Milford, MA, USA). The injection volume was 5 µL and the flow rate was adjusted to 0.3 ml min^{-1} using an Agilent 1200 Series HPLC System. The chromatographic system was coupled to an Agilent 8900 Triple Quadrupole ICP-MS/MS instrument (Agilent Technologies, Santa Clara, CA, USA). The instrument was operated in MS/MS mode using oxygen (99.995%, grade 4.5, North Ryde, NSW, Australia) as cell gas for mass shifting of sulphur. The performance of the ICP-MS instrument was tuned daily with a solution containing 1 µg L^{-1} Li, Y, Tl and Ce to optimise sensitivity. The tune parameters for mass-shifting were optimised analysing a 200 ng g^{-1} sulphur standard. The plasma was operated at 1.6 kW, oxygen was used as cell gas (18 %) and the typical nebuliser gas flow rate was 1.04 L min^{-1}.

LA-ICP-MS experiments were performed with a New Wave Research NWR193 laser ablation system (New Wave Research, Fremont, CA, USA), coupled to an Agilent 7900 ICP-MS (Agilent Technologies, Santa Clara, CA, USA). The LA-ICP-MS was tuned for maximum sensitivity before each measurement using the reference material NIST 612 "Trace Elements in Glass". Typical instrument parameters are outlined in Table 1. Images were analysed and created with the open source imaging software, pew^2 1.2.1.[29]

H&E images were analysed with a ZEISS AxioScan Z.1 slide scanner (Carl Zeiss AG, Oberkochen, Germany).

Antibody characterisation

Table 1. Operating conditions for the ICP-MS and laser ablation system.

Agilent 7900 ICP-MS	
RF Power	1550 W
Nebuliser Gas	1.04 L min^{-1}
Isotopes	^{142}Nd, ^{170}Er, ^{31}P, ^{13}C, ^{56}Fe, ^{63}Cu, ^{66}Zn
Integration times	0.1 s (Nd, Er), 0.01 s (P, C, Fe, Cu, Zn)

NWR193 LA System	
Laser wavelength	193 nm
Fluence	20% (3 J/cm^2)
Repetition rate	20 Hz
Spot size	35 µm
Scan speed	140 µm s^{-1}

Labelled antibodies were characterised by a double on-line isotope dilution SEC-ICP-MS method previously described by Clases *et al*. [25] A spike solution was continuously introduced (at 0.4 mL/min) through a T-piece. The spike solution contained a ^{34}S isotope-enriched standard (200 ng g^{-1}), for IDA of the sulphur integral to the antibodies and standards of Nd and Er with natural isotopic abundances (1 µg g^{-1}) for reverse IDA of the isotopically enriched MAXPAR® labels. Experimental isotopic abundances of both spikes and samples were determined by off-line ICP-MS/MS to consider instrumental mass bias. The detector's deadtime was determined and corrected by the analysis software (MassHunter, Agilent Technologies) analysing a diluted Er standard. Quantitative information was obtained following the integration of the mass flow signals using R and RStudio and presented using OriginPro 2017 software (v8.0724, Microcal Software Inc., Northampton, MA, USA).

Immunohistochemistry optimisations

Several figures depicting the immunohistochemistry optimisation are provided in Figure S1. To optimise contrasts, antibody titrations were performed using dilutions 1:100 and 1:500. In both cases anti-MMP-11 and anti-CD45, the 1:100 dilution provided improved contrast; however, high unspecific background staining was evident (Figure S1). This was corrected by decreasing the incubation period to 1 hour and by application of a thresholding algorithm to remove background levels from statistical analyses.

Multiplexing was achieved via sequential incubations of anti-MMP-11 and anti-CD45. The multiplexed method resulted in decreased staining of anti-CD45, as such, the dilution of anti-CD45 was finally adjusted to 1:50. The reproducibility of the multiplexed staining method was qualitatively assessed by comparison of three stained semi-consecutive breast cancer tissue sections and LA-ICP-MS analyses produced comparable element distributions. Example figures depicting immunohistochemistry optimisation are provided is Figure S1. Elemental LA-ICP-MS images for Fe, Cu and Zn obtained simultaneously from immunohistochemically stained breast cancer tissue sections are showed in Figure S2. However, the application of dewaxing, washing and incubations steps corrupted the distribution of endogenous elements due to wash-out effects as well as contaminations (compare Figure S2). This pertained the simultaneous analysis and comparison of protein and endogenous element distributions.

Calibration strategy

External calibration using mould-prepared gelatine standards was performed following the protocol previously described by Westerhausen *et al*. [24]. Calibration curves for Nd and Er were constructed by plotting the signal intensity obtained by LA-ICP-MS vs. the standards concentration (50, 100, 400, 700 and 1000 ng g^{-1}). The exact concentrations of the analytes in the standards were determined by ICP-MS after acid digestion. The mean correlation coefficient of the calibration curves was 0.981 (RSD of 2.72%) across all measurements. Each data point for the subsequent analyses was then converted to concentration using linear regression equation of the corresponding calibration curve of the respective element.

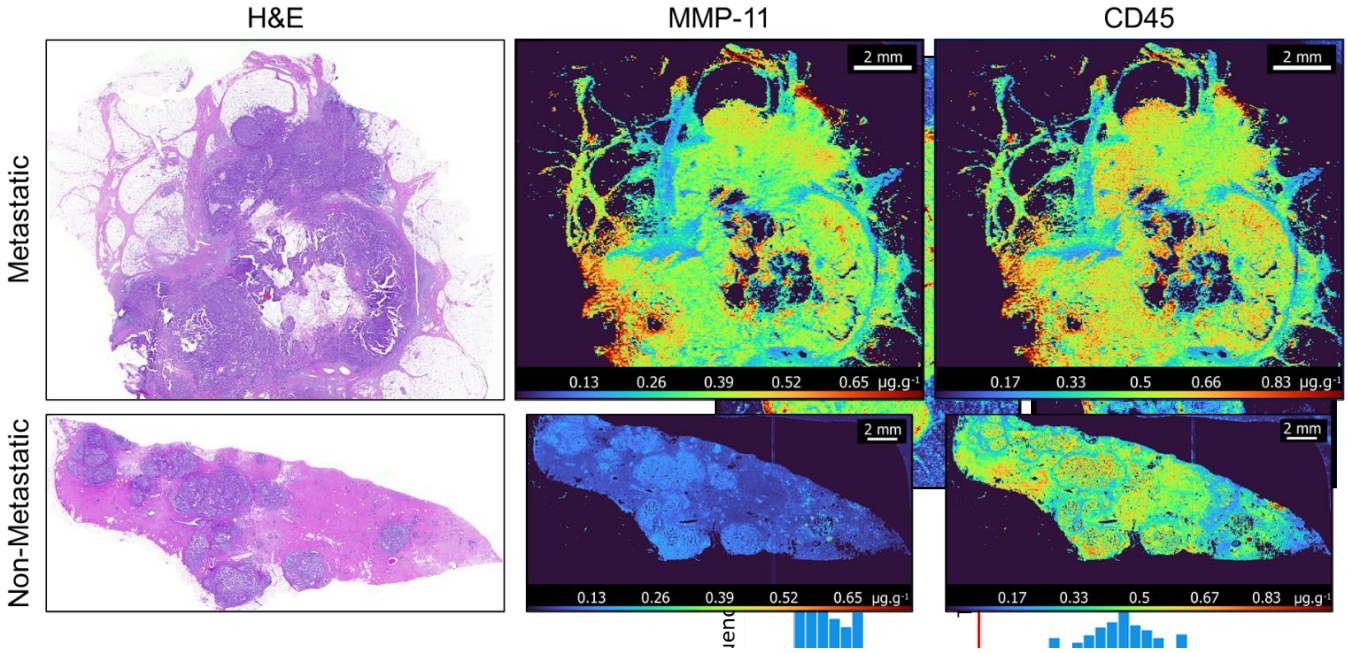

Figure 3. Exemplar images of metastatic (top) and non-metastatic (bottom) breast cancer tissue samples. **Left -** Images of H&E-stained consecutive tissue sections. **Centre** - Quantified LA-ICP-MS images of MMP-11 distribution. **Right -** Quantified LA-ICP-MS images of CD45 distribution. Background removed by *k*-means based thresholding.

Statistical analysis

OriginPro 2017 was used to assess the significance of differences between factors with paired or unpaired, two-tailed t-tests at a 95% confidence interval and equal variances not assumed.

k-means clustering, an algorithmic process which involves vectorisation of the data followed by calculation of *k* centroids, was used for image segmentation, and completed using functions of pew[2] 1.2.1 [29,30].

Results and Discussion

Antibody characterisation and image thresholding

The metal loading content of MaxPar™ polymers depends upon the detailed and nuanced preparation steps outlined by the manufacturer (reference protocol here) and is likely to be variable each time the procedure is undertaken. Knowledge of the number of metal atoms per antibody was also required to enable repeatable analysis by LA-ICP-MS. Accordingly, the metal load of anti-MMP-11 and anti-CD45 was characterised by concomitant quantification of S and the respective metal tag using SEC-ICP-MS/MS and double on-line IDA [25]. Here, the number of S atoms in the primary structure of the antibodies (IgG_1: 32 S atoms, IgG_{2B}: 36 S atoms for anti-CD45 and anti-MMP-11, respectively) enabled calculations of the molar labelling ratio. The selective analysis of S required mass shifting to mitigate obscuration by polyatomic interferences such as $^{16}O_2^+$, $^{14}N^{18}O^+$, $^{15}N^{17}O^+$, $^{14}N^{17}O^1H^+$ [31]. Figure 1a details a typical intensity chromatogram obtained by SEC-IDA-ICP-MS/MS of anti-MMP-11 labelled with isotopically enriched ^{142}Nd. S was quantified by post column addition of enriched ^{34}S, whilst Nd was quantified with naturally abundant Nd. Figure 1b shows the S and Nd mass flow analysis which was calculated from transient isotopes ratios. Integration of the latter mass flow chromatogram provided the absolute mass of S and Nd in the injected volume, which translated to 104.0 and 112.2 average number of

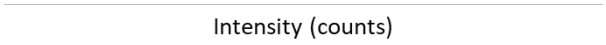

Figure 2. Example of background removal using '*k*-means clustering' based segmentation on an LA-ICP-MS image. **(a)** Image before background removal, **(b)** image after background removal, **(c)** histogram visualisation of threshold.

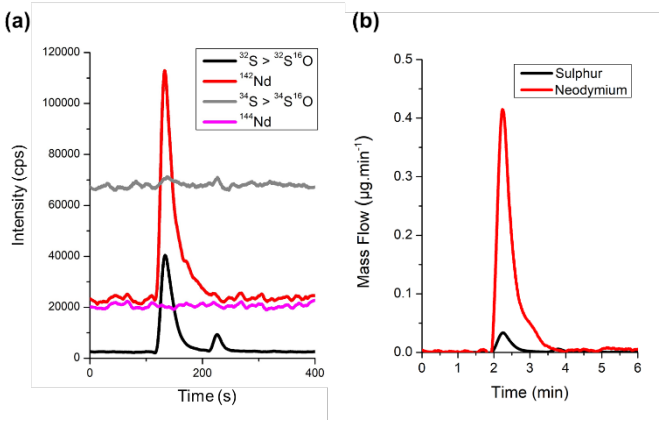

Figure 1. (a) Intensity chromatograms obtained by SEC-IDA-ICP-MS/MS analysis of ^{142}Nd labelled anti-MMP-11. **(b)** Mass flow chromatogram of the same labelled antibody, calculated by isotope dilution analysis.

lanthanide atoms per anti–MMP-11 and anti-CD45, respectively. Furthermore, the antibody concentration was 0.38 mg mL^{-1} for anti-MMP-11 and 0.65 mg mL^{-1} for anti-CD45. These values were consistent with the approximate expected recovery of 60% for the MAXPAR® labelling process.

These characterised antibodies were subsequently used in IHC-protocols, analysed by LA-ICP-MS, and quantified via external calibration. The labelling degree was used to translate the lanthanide concentration into the corresponding antibody concentration. As the monoclonal antibodies solely bind to one specific epitope of the biomarkers, the antibody mass concentrations

provided a direct representation of MMP-11 and CD45 concentrations.

In quantitative image analysis, analysed regions outside of tissue areas or holes within the specimens lead to biased results and corresponding pixels must be removed prior to statistical analyses [32]. Common segmentation methods include, median, Otsu's method, *k*-medians, and *k*-means enabling recognition and masking of non-tissue areas [33]. In this study a *k*-means clustering method (k = 3) was employed to set a threshold under which a pixel was recognised as non-tissue area and masked as shown in Figure 2, k = 3 was chosen based on the 'elbow method' described by Castellanos-Garcia *et al*.[30], and allows for segmentation between background, low concentration, and high concentration areas. Figure 2a shows the raw ^{142}Nd intensity in a non-metastatic breast cancer tissue stained with ^{142}Nd labelled anti-MMP-11. While tissue areas and margins are clearly visible, it is obvious that ignoring unspecific background staining areas outside the tissue would lead to an inaccurate quantitative interpretation. Figure 2c shows the ^{142}Nd intensity histogram of the image containing two signal populations. These populations correspond to unspecific background staining outside the tissue area (left) and the MMP-11 specific staining (right). In this example the k-means clustering threshold was determined to be 58 counts and pixels with intensities below this threshold were excluded from further analysis as displayed in Figure 2b.

Role of MMP11 and CD45 in breast cancer tissues

The characterised labelled antibodies were subsequently employed to investigate the quantitative spatial distribution of MMP-11 and CD45 in breast cancer tissues. Cu, Fe and Zn were acquired simultaneously to evaluate possible co-localisations with tumour areas. Distributions of Cu, Fe, and Zn distribution are shown in Figure S2. While there was an upregulation of these metals in tumour areas, there is no evidence of co-localisation with MMP-11 and CD45. However, it is likely that native element distributions were impacted by paraffination, deparaffinization and washing steps limiting both qualitative and quantitative analyses.

Spatially resolved concentrations of MMP-11 and CD45 were determined in metastatic (n = 12), non-metastatic (n = 9) and healthy breast tissue samples (n = 4). Figure 3 shows the quantitative distribution of MMP-11 (centre) and CD45 (right) in one representative metastatic (top) and one representative non-metastatic samples (bottom). This example in figure 3 demonstrates that there was no notable link between metastasis and the expression of CD45, however, MMP-11 was significantly upregulated in metastatic breast tissue. It is noteworthy, that areas with high concentration of CD45 showed high concentration of MMP11, which was related with a poor prognostic in breast cancer patients (refs PMID: 31342542, 26140253). Furthermore, metastatic samples contained more heterogenous MMP-11 distributions throughout the tumour microenvironment with concentrations values reaching up to 0.65 µg g^{-1} (see Figure 3 centre). This observation was consistent across the entire sample set and is in line with a previous study on the distribution of MMP-11 in a smaller cohort [14]. Comparison to the complementary H&E images allowed identification of different tissues and indicated that MMP-11 was overexpressed in stroma and tumour cells around the margins of large metastatic tumours. This is consistent with the role of MMP-11 as a factor involved in the degradation of the extracellular matrix. However, MMP-11 distribution in non-metastatic breast cancer tissues was more homogenous indicating that MMP-11 may play essential roles during invasion and metastatic processes. CD45 was mostly localised in tumour areas with high cell densities and, unlike MMP-11, less in the adjacent stromal areas. This is plausible as CD45 as a transmembrane protein was expected to be more abundant in areas of high cell density.

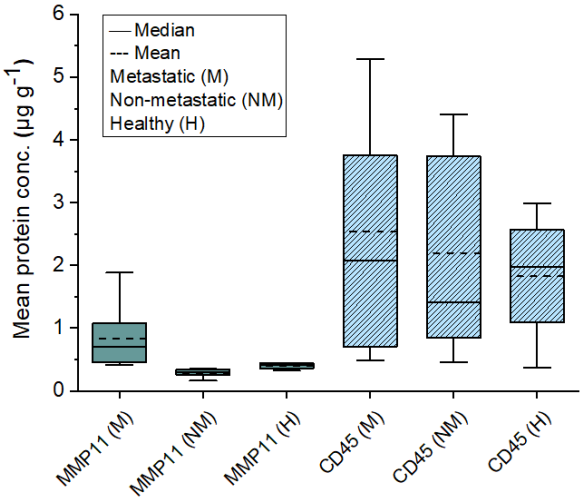

Figure 4 Mean protein concentration of MMP-11 and CD45 obtained for metastatic (n=12), non-metastatic (n=9) and healthy breast tissue sections (n = 4).

Across all samples (see Table S1), CD45 concentrations ranged from 0.45 ± 0.40 µg g^{-1} to 5.28 ± 1.43 µg g^{-1} and no significant differences between metastatic (mean: 2.54 ± 1.62 µg g^{-1}) and non-metastatic (mean: 2.20 ± 1.60 µg g^{-1}, p = 0.70), or metastatic and healthy specimens (mean: 1.83 ± 0.95 µg g^{-1}, p = 0.42) were determined (compare Figure 4). However, MMP-11 was significantly increased by up to factor 3 (up to 202% increment) in metastatic tissues compared to non-metastatic (p = 0.0016) and healthy tissues (p = 0.0077). Healthy breast tissues analysed showed a significant increase of 43.5% compared to non-metastatic tissue for MMP-11 (p = 0.0087). The mean concentration across all metastatic samples was 0.74 ± 0.41 µg g^{-1}, across non-metastatic samples 0.25 ± 0.06 µg g^{-1} and across tissues from healthy patients 0.35 ± 0.05 µg g^{-1}.

Additional comparison between MMP-11 and CD45 concentrations among the studied groups was assessed by performing a paired t-test and determining the Pearson correlation coefficient (r). MMP-11 and CD45 concentrations obtained for non-metastatic tissues are significant different (p = 0,008) with a Pearson coefficient of 0,15, indicating no correlation between these two variables in the studied group. Nevertheless, a positive correlation between MMP-11 and CD45 was found (r = 0,93) within the metastatic group with a p value of 0,01, demonstrating that when the MMP-11 concentration increases also does the CD45.

For further comparison routine colorimetric IHC testing were performed for MMP-11, PR, ER, and HER2 and graded as positive (1) or negative (0) to investigate correlations to concentrations of MMP-11 determined via IHC-assisted LA-ICP-MS (see Table S1). However, there was no significant link between PR, ER and HER2 gradings and concentrations of MMP-11 (p > 0.15), which underpins the utility of MMP-11 as a prognostic factor providing complementary clinical data.

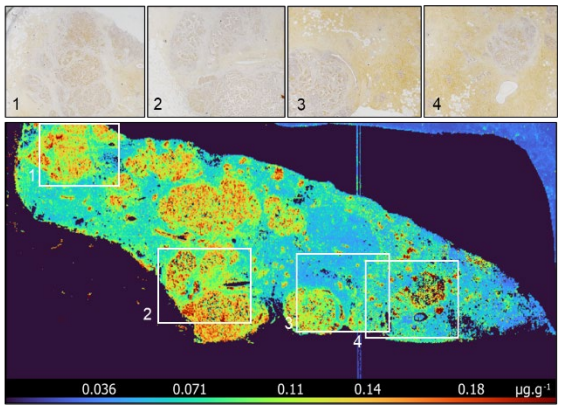

Figure 5. Visualisation of MMP11in a non-metastatic breast cancer tissue by immunohistochemically-assisted LA-ICP-MS compared against traditional IHC staining.

Additionally, in figure 5 the result of traditional IHC testing for MMP-11 was compared against the immunohistochemistry-assisted LA-ICP-MS method. The comparison shows a distribution which is consistent between both methods, with an advantage of the LA-ICP-MS method being a significant increase in sensitivity [34] allowing for more graduation and detailed analysis. Furthermore, quantitative analysis is useful for objective grading, alleviating concerns with visual grading, and providing important additional information to traditional IHC techniques.

Conclusions

A multiplexed immunohistochemistry-assisted LA-ICP-MS method was developed to visualise and quantify the distribution of MMP-11 and CD45 in metastatic tumour tissues, non-metastatic tumour tissues and in control samples. Lanthanide polymer tags were conjugated to corresponding antibodies and to enable quantitative analysis, labelled antibodies were characterised by SEC-ICP-MS/MS using a double on-line IDA approach to determine exact antibody concentrations and labelling degrees. A staining procedure was developed and raw intensities from labelled antibodies as proxy for the targeted biomarkers were calibrated using mould-prepared lanthanide spiked gelatine standards. Furthermore, *k*-means clustering algorithm was used to selectively investigate tissue areas while masking unspecific background staining.

CD45 was expressed in high cell density areas of tumours, however, no significant difference between metastatic, non-metastatic and control samples were found. On the other hand, MMP-11 was significantly overexpressed in the microenvironment of metastatic tumours tissues (mean: 0.74 ± 0.41 µg g^{-1}) compared to both healthy (mean: 0.35 ± 0.05 µg g^{-1}, $p = 0.0016$) and non-metastatic tissue samples (mean: 0.25 ± 0.06 µg g^{-1}, $p = 0.0077$).

This study demonstrates the utility of IHC-assisted LA-ICP-MS as well as dedicated characterisation steps to accomplish quantitative imaging of bio-indicative proteins. The high sensitivity and resolution of LA-ICP-MS were specifically useful to probe the tumour microenvironment and to provide more nuanced data of protein expressions levels and for statistical models to objectively point out differences between various cohorts.

Author Contributions

The manuscript was written through contributions of all authors. All authors have given approval to the final version of the manuscript.

CRediT Author Statement

Dylan Johnson: Methodology, Validation, Formal analysis, Investigation, Writing - Original Draft **David Clases:** Conceptualisation, Methodology, Visualisation, Writing - Review & Editing **Maria Luisa Fernandez-Sanchez:** Conceptualisation, Writing - Review & Editing **Noemi Eiró:** Investigation, Writing - Review & Editing **Luis O. Gonzalez:** Investigation, Writing - Review & Editing **Francisco J. Vizoso:** Resources, Writing - Review & Editing **Philip A. Doble:** Resources, Writing - Review & Editing **Raquel Gonzalez de Vega:** Conceptualisation, Methodology, Investigation, Visualisation, Supervision, Writing - Review & Editing

Acknowledgment

DJ is supported by an Australian Government Research Training Program Stipend. PAD is supported by Australian Research Council Discovery Project Grant (DP190102361). MFS is supported by the Spanish Ministry of Economy and Competitiveness through the project PID2019-109698G-I00.

The Agilent 7900 ICP-MS is a loan instrument provided by Agilent Australia for research use.

Conflict of Interest

The authors declare no conflicts of interest.

References

[1] H. Sung, J. Ferlay, R.L. Siegel, M. Laversanne, I. Soerjomataram, A. Jemal, F. Bray, Global Cancer Statistics 2020: GLOBOCAN Estimates of Incidence and Mortality Worldwide for 36 Cancers in 185 Countries, CA Cancer J Clin. 71 (2021) 209–249. https://doi.org/10.3322/caac.21660.

[2] C. DeSantis, J. Ma, L. Bryan, A. Jemal, Breast cancer statistics, 2013, CA: A Cancer Journal for Clinicians. 64 (2014) 52–62. https://doi.org/10.3322/caac.21203.

[3] E. Mallon, P. Osin, N. Nasiri, I. Blain, B. Howard, B. Gusterson, The Basic Pathology of Human Breast Cancer, Journal of Mammary Gland Biology and Neoplasia. 5 (2000) 139–163. https://doi.org/10.1023/a:1026439204849.

[4] N. Patani, L.-A. Martin, M. Dowsett, Biomarkers for the clinical management of breast cancer: International perspective: Biomarkers of breast cancer, Int. J. Cancer. 133 (2013) 1–13. https://doi.org/10.1002/ijc.27997.

[5] B. Davidson, R. Reich, B. Risberg, J.M. Nesland, The biological role and regulation of matrix metalloproteinases (MMP) in cancer, Arkh Patol. 64 (2002) 47–53.

[6] X. Zhang, S. Huang, J. Guo, L. Zhou, L. You, T. Zhang, Y. Zhao, Insights into the distinct roles of MMP-11 in tumor biology and future therapeutics (Review), Int. J. Oncol. 48 (2016) 1783–1793. https://doi.org/10.3892/ijo.2016.3400.

[7] Matrix metalloproteinase stromelysin-3 in development and pathogenesis, Histology and Histopathology. (2005) 177–185. https://doi.org/10.14670/HH-20.177.

[8] S. Frisch, H. Francis, Disruption of epithelial cell-matrix interactions induces apoptosis, The Journal of Cell Biology. 124 (1994) 619–626. https://doi.org/10.1083/jcb.124.4.619.

[9] P. Basset, J.P. Bellocq, C. Wolf, I. Stoll, P. Hutin, J.M. Limacher, O.L. Podhajcer, M.P. Chenard, M.C. Rio, P. Chambon, A novel metalloproteinase gene specifically expressed in stromal cells of breast carcinomas, Nature. 348 (1990) 699–704. https://doi.org/10.1038/348699a0.

[10] J.I. Barrasa, N. Olmo, A. Santiago-Gómez, E. Lecona, P. Anglard, J. Turnay, M.A. Lizarbe, Histone deacetylase inhibitors upregulate MMP11 gene expression through Sp1/Smad complexes in human colon adenocarcinoma cells, Biochimica et Biophysica Acta (BBA) - Molecular Cell Research. 1823 (2012) 570–581. https://doi.org/10.1016/j.bbamcr.2011.12.010.

[11] A. Köhrmann, U. Kammerer, M. Kapp, J. Dietl, J. Anacker, Expression of matrix metalloproteinases (MMPs) in primary human breast cancer and breast cancer cell lines: New findings and review of the literature, BMC Cancer. 9 (2009) 188. https://doi.org/10.1186/1471-2407-9-188.

[12] K.-W. Min, D.-H. Kim, S.-I. Do, J.-S. Pyo, K. Kim, S.W. Chae, J.H. Sohn, Y.-H. Oh, H.J. Kim, S.H. Choi, Y.J. Choi, C.H. Park, Diagnostic and Prognostic Relevance of MMP-11 Expression in the Stromal Fibroblast-Like Cells Adjacent to Invasive Ductal Carcinoma of the Breast, Ann Surg Oncol. 20 (2013) 433–442. https://doi.org/10.1245/s10434-012-2734-3.

[13] R. González de Vega, M.L.F. Sanchez, N. Eiro, F.J. Vizoso, M. Sperling, U. Karst, A.S. Medel, Multimodal laser ablation/desorption imaging analysis of Zn and MMP-11 in breast tissues, Anal Bioanal Chem. 410 (2018) 913–922. https://doi.org/10.1007/s00216-017-0537-x.

[14] R. González de Vega, D. Clases, M.L. Fernández-Sánchez, N. Eiró, L.O. González, F.J. Vizoso, P.A. Doble, A. Sanz-Medel, MMP-11 as a biomarker for metastatic breast cancer by immunohistochemical-assisted imaging mass spectrometry, Anal Bioanal Chem. 411 (2019) 639–646. https://doi.org/10.1007/s00216-018-1365-3.

[15] N. Eiro, S. Cid, B. Fernández, M. Fraile, A. Cernea, R. Sánchez, A. Andicoechea, E.J.D. Galiana, L.O. González, Z. Fernández-Muñiz, J.L. Fernández-Martínez, F.J. Vizoso, MMP11 expression in intratumoral inflammatory cells in breast cancer, Histopathology. 75 (2019) 916–930. https://doi.org/10.1111/his.13956.

[16] N. Holmes, CD45: all is not yet crystal clear, Immunology. 117 (2006) 145–155. https://doi.org/10.1111/j.1365-2567.2005.02265.x.

[17] C.W. Caldwell, W.P. Patterson, Relationship between CD45 antigen expression and putative stages of differentiation in B-cell malignancies, Am. J. Hematol. 36 (1991) 111–115. https://doi.org/10.1002/ajh.2830360209.

[18] B. Ruffell, A. Au, H.S. Rugo, L.J. Esserman, E.S. Hwang, L.M. Coussens, Leukocyte composition of human breast cancer, PNAS. 109 (2012) 2796–2801. https://doi.org/10.1073/pnas.1104303108.

[19] M.L. Hermiston, Z. Xu, A. Weiss, CD45: A Critical Regulator of Signaling Thresholds in Immune Cells, Annual Review of Immunology. 21 (2003) 107–137. http://dx.doi.org.ezproxy.lib.uts.edu.au/10.1146/annurev.immunol.21.120601.140946.

[20] R.A. Walker, Quantification of immunohistochemistry issues concerning methods, utility and semiquantitative assessment I, Histopathology. 49 (2006) 406–410. https://doi.org/10.1111/j.1365-2559.2006.02514.x.

[21] P.A. Doble, R.G. de Vega, D.P. Bishop, D.J. Hare, D. Clases, Laser Ablation–Inductively Coupled Plasma–Mass Spectrometry Imaging in Biology, Chem. Rev. (2021). https://doi.org/10.1021/acs.chemrev.0c01219.

[22] D. P. Bishop, D. Clases, F. Fryer, E. Williams, S. Wilkins, D. J. Hare, N. Cole, U. Karst, P. A. Doble, Elemental bio-imaging using laser ablation-triple quadrupole-ICP-MS, Journal of Analytical Atomic Spectrometry. 31 (2016) 197–202. https://doi.org/10.1039/C5JA00293A.

[23] R.G. de Vega, M.L. Fernández-Sánchez, J. Pisonero, N. Eiró, F.J. Vizoso, A. Sanz-Medel, Quantitative bioimaging of Ca, Fe, Cu and Zn in breast cancer tissues by LA-ICP-MS, J. Anal. At. Spectrom. 32 (2017) 671–677. https://doi.org/10.1039/C6JA00390G.

[24] M.T. Westerhausen, T.E. Lockwood, R. Gonzalez de Vega, A. Röhnelt, D.P. Bishop, N. Cole, P.A. Doble, D. Clases, Low background mould-prepared gelatine standards for reproducible quantification in elemental bio-imaging, Analyst. 144 (2019) 6881–6888. https://doi.org/10.1039/C9AN01580A.

[25] D. Clases, R.G. de Vega, P.A. Adlard, P.A. Doble, Online reverse isotope dilution analysis for spatial quantification of elemental labels used in immunohistochemical assisted imaging mass spectrometry via LA-ICP-MS, J. Anal. At. Spectrom. 34 (2019) 407–412. https://doi.org/10.1039/C8JA00324F.

[26] B. Paul, D.J. Hare, D.P. Bishop, C. Paton, V.T. Nguyen, N. Cole, M.M. Niedwiecki, E. Andreozzi, A. Vais, J.L. Billings, L. Bray, A.I. Bush, G. McColl, B.R. Roberts, P.A. Adlard, D.I. Finkelstein, J. Hellstrom, J.M. Hergt, J.D. Woodhead, P.A. Doble, Visualising mouse neuroanatomy and function by metal distribution using laser ablation-inductively coupled plasma-mass spectrometry imaging, Chem. Sci. 6 (2015) 5383–5393. https://doi.org/10.1039/C5SC02231B.

[27] D. Clases, R. Gonzalez de Vega, S. Funke, T.E. Lockwood, M.T. Westerhausen, R.V. Taudte, P.A. Adlard, P.A. Doble, Matching sensitivity to abundance: high resolution immuno-mass spectrometry imaging of lanthanide labels and endogenous elements in the murine brain, J. Anal. At. Spectrom. 35 (2020) 728–735. https://doi.org/10.1039/C9JA00405J.

[28] M.E. Ijsselsteijn, R. van der Breggen, A. Farina Sarasqueta, F. Koning, N.F.C.C. de Miranda, A 40-Marker Panel for High Dimensional Characterization of Cancer Immune Microenvironments by Imaging Mass Cytometry, Frontiers in Immunology. 10 (2019) 2534. https://doi.org/10.3389/fimmu.2019.02534.

[29] T.E. Lockwood, M.T. Westerhausen, P.A. Doble, Pew2: Open-Source Imaging Software for Laser Ablation–Inductively Coupled Plasma–Mass Spectrometry, Anal. Chem. (2021). https://doi.org/10.1021/acs.analchem.1c02138.

[30] L.J. Castellanos-García, S.G. Elci, R.W. Vachet, Reconstruction, analysis, and segmentation of LA-ICP-MS imaging data using Python for the identification of sub-organ regions in tissues, Analyst. 145 (2020) 3705–3712. https://doi.org/10.1039/C9AN02472G.
[31] T.W. May, R.H. Wiedmeyer, A table of polyatomic interferences in ICP-MS, ATOMIC SPECTROSCOPY. 19 (1998) 150–155.
[32] M.M. Niedzwiecki, C. Austin, R. Remark, M. Merad, S. Gnjatic, G. Estrada-Gutierrez, A. Espejel-Nuñez, H. Borboa-Olivares, M. Guzman-Huerta, R.J. Wright, R.O. Wright, M. Arora, A multimodal imaging workflow to visualize metal mixtures in the human placenta and explore colocalization with biological response markers†, Metallomics. 8 (2016) 444–452. https://doi.org/10.1039/c6mt00010j.
[33] D.P. Bishop, M.T. Westerhausen, F. Barthelemy, T. Lockwood, N. Cole, E.M. Gibbs, R.H. Crosbie, S.F. Nelson, M.C. Miceli, P.A. Doble, J. Wanagat, Quantitative immuno-mass spectrometry imaging of skeletal muscle dystrophin, Sci Rep. 11 (2021) 1128. https://doi.org/10.1038/s41598-020-80495-8.
[34] R.M. Levenson, A.D. Borowsky, M. Angelo, Immunohistochemistry and mass spectrometry for highly multiplexed cellular molecular imaging, Lab Invest. 95 (2015) 397–405. https://doi.org/10.1038/labinvest.2015.2.